International Journal of Engineering Innovation & Research
Volume 15, Issue 6, ISSN: 2277 – 5668

Hybrid Transformer and Convolutional Neural Network Surrogate with Adaptive Quantum Binary Particle Swarm Optimization for Dual-Band Microstrip Antenna Design

Lakshmi Ganabathy A.
M.Tech Scholar (Communication Systems), Department of Electronics and Communication Engineering, Ponnaiyah Ramajayam Institute of Science and Technology (PRIST) Deemed to be University, Thanjavur, Tamil Nadu, India.
Corresponding author email id: lakshmiganabathy.a@gmail.com

Date of publication (dd/mm/yyyy): 05/11/2026

***Abstract* – Aim: To move beyond manual tuning and parameter sweeps inside full-wave solvers through automated refinement and multi-objective design at four times the pixel count. Methods: A dual-band T-shaped microstrip antenna on a 70 mm × 45 mm × 1.6 mm FR4 substrate is modelled in ANSYS HFSS. The radiating region is encoded as a 20 × 20 binary pixel matrix with 400 design variables. A hybrid surrogate uses convolutional layers to extract local geometric features and a Vision Transformer encoder to model long-range coupling across the patch. The surrogate jointly predicts reflection coefficient, gain, radiation efficiency, VSWR and bandwidth. Adaptive Quantum Binary Particle Swarm Optimization (AQBPSO), combined with NSGA-II non-dominated sorting, returns Pareto-optimal geometries. Physics-informed penalties for symmetry, connectivity and feed contact keep the synthesized layouts manufacturable. Results: The antenna resonates at 3.4125 GHz and 5.0125 GHz, with reflection coefficients of −19.36 dB and −22.45 dB, respectively. The −10 dB bandwidths are approximately 3.27–3.55 GHz and 4.81–6.64 GHz, with VSWR below 1.25 at both resonances. The framework achieves an estimated 35–45 fold reduction in design time relative to direct full-wave optimization.**

***Keywords* – Dual-Band Microstrip Antenna, Inverse Design, Pixelated Antenna, Convolutional Neural Network (CNN), Vision Transformer (ViT), Adaptive Quantum Binary Particle Swarm Optimization (AQBPSO), NSGA-II, Sub-6 GHz 5G, WLAN.**

I. INTRODUCTION

Wireless traffic now flows through a dense mix of cellular, local-area and machine-type links, and a single handheld or Internet of Things (IoT) node is often expected to operate on several of them at once. The 3.3-3.8 GHz range has become the principal mid-band allocation for 5G New Radio [1], while the 5 GHz region continues to carry most high-throughput WLAN traffic [2]. Supporting both with one radiator, rather than two separate antennas, saves board area, reduces feed-network complexity and lowers cost, which makes compact dual-band antennas a practical necessity for modern terminals [3].

Microstrip patch antennas are the usual starting point for such designs because they are planar, light, inexpensive to fabricate on printed circuit boards and easy to integrate with front-end electronics [4], [5]. Their best-known weaknesses are a narrow impedance bandwidth, modest gain and, in the basic rectangular form, a single resonance. A large body of work has extended the patch concept through series feeding, dual polarization, differential feeds, complementary radiators and array configurations [6] Multi-band behaviour is commonly obtained by reshaping the radiator, for example with slots, stubs or branched arms, so that more than one current path resonates within a fixed footprint. The T-shaped radiator is attractive in this respect: its stem and its two horizontal arms offer two distinct path lengths that can be tuned with relatively few parameters.

Copyright © 2026 IJEIR, All right reserved

Even for simple geometries, however, the conventional workflow is iterative. An initial layout is derived from closed-form equations, simulated with a full-wave solver such as ANSYS HFSS or CST Studio Suite, and then adjusted by hand until the targets are met. Each solver run can take minutes to hours, and when gain, efficiency and bandwidth must be balanced together the number of runs grows rapidly [12]. Machine learning has therefore been adopted to build fast surrogate models of antenna behaviour [13]. Inverse neural networks and tandem networks have been used to map performance targets back to geometry [15], convolutional networks have been trained on pixelated layouts [17], deep-learning inverse design has been extended to millimetre-wave passive structures [19], and generative models have been used to enlarge scarce training sets [20].

A recent framework discretized the patch into a 10 × 10 binary grid, trained a convolutional neural network (CNN) on simulated samples to predict the reflection coefficient S_{11}, and coupled it with Binary Particle Swarm Optimization (BPSO), reporting roughly a 25-fold acceleration over direct solver-in-the-loop optimization [21]. That approach demonstrates the value of pixel-level freedom, but it leaves four gaps: (a) only S_{11} is optimized, so gain, efficiency and bandwidth are not controlled; (b) 100 pixels limit how finely current paths can be shaped; (c) a pure CNN has a limited receptive field and does not explicitly model coupling between distant regions of the patch; and (d) standard BPSO tends to lose diversity and converge prematurely in high-dimensional binary spaces.

This paper responds to those gaps in two parts. First, a dual-band T-shaped microstrip antenna for 3.4 GHz and 5.0 GHz operation is designed and characterized in HFSS to establish a physically verified reference. Second, a multi-objective inverse design framework is formulated around that reference. The main contributions are as follows.

(i) A dual-band T-shaped microstrip antenna on low-cost FR4 is presented, with simulated resonances at 3.4125 GHz and 5.0125 GHz suitable for 5G n78 and 5 GHz WLAN use.

(ii) The radiating area is represented as a 20 × 20 pixel matrix, giving 2^{400} candidate layouts and four times the geometric resolution of the 10 × 10 baseline.

(iii) A hybrid CNN–Vision Transformer surrogate is specified that combines local feature extraction with global self-attention and predicts S_{11}, gain, radiation efficiency, VSWR and bandwidth through shared multi-output heads.

(iv) An AQBPSO search with an adaptive contraction–expansion coefficient is coupled with NSGA-II ranking to obtain Pareto-optimal trade-offs, and physics-informed penalties are added so that synthesized layouts remain connected, symmetric and fabricable.

The remainder of the paper is organized as follows. Section II reviews related work. Section III describes the T-shaped antenna design and simulation set-up. Section IV presents the proposed inverse design framework. Section V discusses the simulated results and the expected framework performance, and Section VI concludes the paper.

II. Related Work

A. *Surrogate-Assisted Antenna Design*

Early machine learning work in electromagnetics used artificial neural networks, support vector regression a-

Copyright © 2026 IJEIR, All right reserved

-d tree-based models to approximate solver output from a handful of geometric parameters [13]. Such models are accurate inside the region spanned by their training data and evaluate in milliseconds, which makes them natural partners for population-based optimizers. Wu *et al.* applied machine-learning-assisted optimization directly to antenna geometry [14], and similar surrogate strategies have been used for multi-band filtering power dividers [22]. A persistent difficulty is that the model must be retrained when the parameterization changes, and parametric models cannot represent shapes outside the chosen template.

B. *Pixelated and Inverse Design*

Pixelated encoding removes the template restriction by letting each cell of a grid be metal or not. Jacobs showed that CNN regression can learn the dual-band response of pixelated microstrip antennas [17], and Karahan *et al.* used deep-learning inverse design to obtain non-intuitive planar antennas and millimetre-wave passives [18]. Inverse networks map specifications to geometry directly [15], while tandem networks address the one-to-many nature of that mapping [16]. The CNN–BPSO framework of [21] is the closest baseline to the present work; Table 1 contrasts it with other representative studies.

Table 1. Summary of representative AI-assisted antenna design studies.

Reference	Technique	Design Variables	Optimized Outputs
[17]	CNN regression	Pixelated patch	Dual-band S_{11}
[15]	Inverse ANN	Parametric	Multiple objectives
[16]	Tandem neural network	Parametric	Multiband response
[18]	Deep-learning inverse design	Pixelated planar	S-parameters
[20]	GAN data augmentation	Parametric	Training data generation
[21]	CNN + BPSO	10 × 10 pixels	S_{11} only
This work	CNN–ViT + AQBPSO–NSGA-II	20 × 20 pixels	S_{11}, gain, efficiency, VSWR, BW

C. *Attention Models and Swarm Search*

Transformers replace convolution with self-attention, allowing every input token to weigh every other token [23]. The Vision Transformer applies this idea to image patches [24], which suits pixelated antennas because a slot at one edge of a patch can shift a resonance governed by the opposite edge. On the optimization side, binary PSO [25] and its quantum-behaved variant [26] have both been applied to discrete design problems, and NSGA-II remains a standard method for extracting Pareto fronts [27]. Physics-informed learning, in which known physical constraints enter the loss function, has been shown to improve generalization when data are limited [28]. The present work brings these components together for dual-band antenna synthesis.

III. Dual-Band T-Shaped Antenna Design

A. *Geometry and Operating Principle*

The reference antenna, shown in Fig. 1, is printed on an FR4 epoxy substrate of 70 mm × 45 mm with a thickness of 1.6 mm. A copper radiator of 0.035 mm thickness is placed on the top face and a copper ground plane on the bottom face. The radiator consists of a vertical stem joined at its upper end to two horizontal arms, forming a T. The stem is excited at the lower substrate edge by a 50 Ω microstrip line terminated in a wave port.

Copyright © 2026 IJEIR, All right reserved

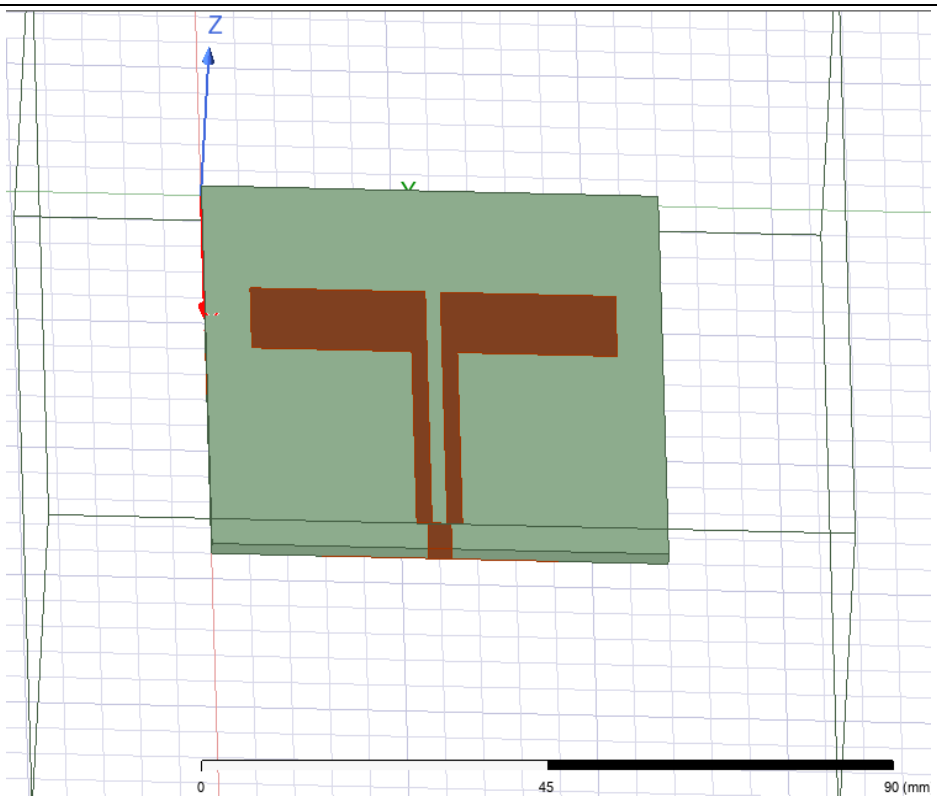


Fig. 1. Geometry of the proposed dual-band T-shaped microstrip antenna modelled in ANSYS HFSS.

The T shape provides two dominant current paths. The longer path, running along the stem and into the arms, sets the lower resonance near 3.4 GHz, while the shorter path associated with the arms produces the upper resonance near 5.0 GHz. Because the two paths share the stem, their resonances can be adjusted largely independently by changing arm length and stem length, without enlarging the substrate.

Initial dimensions were obtained from the transmission-line model of a rectangular patch [5]. For a resonant frequency f_r, substrate permittivity ε_r and thickness h, the patch width W is,

$$W = \frac{c}{2f_r}\sqrt{\frac{2}{\varepsilon_r+1}} \tag{1}$$

and the effective permittivity is

$$\varepsilon_{reff} = \frac{\varepsilon_r+1}{2} + \frac{\varepsilon_r-1}{2}\left(1+\frac{12h}{W}\right)^{-1/2} \tag{2}$$

The fringing-field length extension ΔL and the physical length L follow as

$$\Delta L = 0.412h\,\frac{(\varepsilon_{reff}+0.3)\left(\frac{W}{h}+0.264\right)}{(\varepsilon_{reff}-0.258)\left(\frac{W}{h}+0.8\right)} \tag{3}$$

$$L = \frac{c}{2f_r\sqrt{\varepsilon_{reff}}} - 2\Delta L \tag{4}$$

For the T-shaped branches, each resonance is associated with a current path whose length is close to half a guided wavelength,

$$L_{path,i} \approx \frac{c}{2f_i\sqrt{\varepsilon_{eff}}},\ i = 1,2 \tag{5}$$

Copyright © 2026 IJEIR, All right reserved

where $\varepsilon_{eff} \approx 3.33$ is the effective permittivity of the 50 Ω line on 1.6 mm FR4. Equations (1)-(5) give the starting values listed in Table 2; the stem and arm dimensions were then refined by parametric sweeps in HFSS until both resonances were located at the target frequencies.

Table 2. Substrate data and calculated starting dimensions.

Parameter	Symbol	Value
Substrate material	—	FR4 epoxy
Relative permittivity	ε_r	4.4
Substrate size (L × W × h)	—	70 × 45 × 1.6 mm
Copper thickness	t	0.035 mm
50 Ω microstrip feed width (calculated)	W_f	≈ 3.08 mm
Rectangular-patch width at f_1 = 3.4125 GHz, from (1)	W	26.73 mm
Rectangular-patch length at f_1, from (2)–(4)	L	20.50 mm
Half guided wavelength at f_1, from (5)	$L_{path,1}$	≈ 24.1 mm
Half guided wavelength at f_2 = 5.0125 GHz, from (5)	$L_{path,2}$	≈ 16.4 mm

B. *Simulation Set-Up*

The antenna was analysed in ANSYS HFSS 2025 R2, which solves Maxwell's equations with the finite element method (FEM). The modelling sequence followed the order substrate, ground plane, T-shaped radiator, microstrip feed, material assignment, radiation box, excitation and solution set-up. An air box was placed approximately one quarter of a free-space wavelength from the antenna and assigned a radiation boundary to emulate open space. The solution frequency was set to 5 GHz, near the upper band, and adaptive meshing was run for 10 to 15 passes with a maximum ΔS of 0.02. An interpolating frequency sweep from 2 GHz to 7 GHz was then used to extract S_{11}, VSWR, gain, surface current and far-field patterns.

IV. Proposed AI-Driven Inverse Design Framework

The manual refinement described above is effective for a single parametric shape but does not scale to richer geometries or to several objectives at once. The framework in Fig. 2 replaces most solver calls with a learnt surrogate and searches the pixel space with a multi-objective swarm. It has three stages: data generation, surrogate modelling and multi-objective search, followed by full-wave verification of the selected design.

A. *Pixelated geometry representation*

The radiating region above the feed is divided into a 20 × 20 grid. Each cell p_{mn} takes the value 1 if it is copper and 0 otherwise, so a layout is the binary matrix.

$$P = [p_{mn}] \in \{0,1\}^{20\times 20} \tag{6}$$

which contains 400 design variables and 2^{400} possible configurations. Fig. 3(a) shows a randomly generated, mirror-symmetric candidate; Fig. 3(b) shows the same candidate after cells not electrically connected to the feed have been removed. This connectivity step is applied both when generating training samples and when screening optimizer outputs, so that floating copper islands never reach the solver.

Copyright © 2026 IJEIR, All right reserved

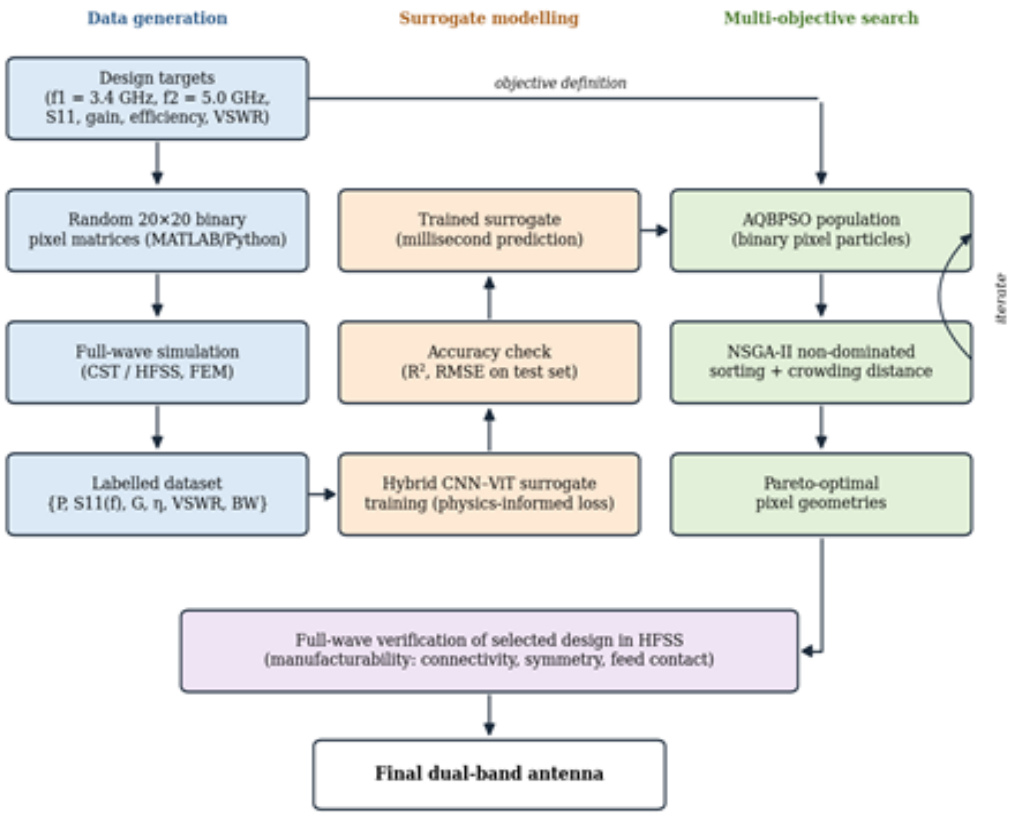


Fig. 2. Workflow of the proposed AI-driven multi-objective inverse design framework.

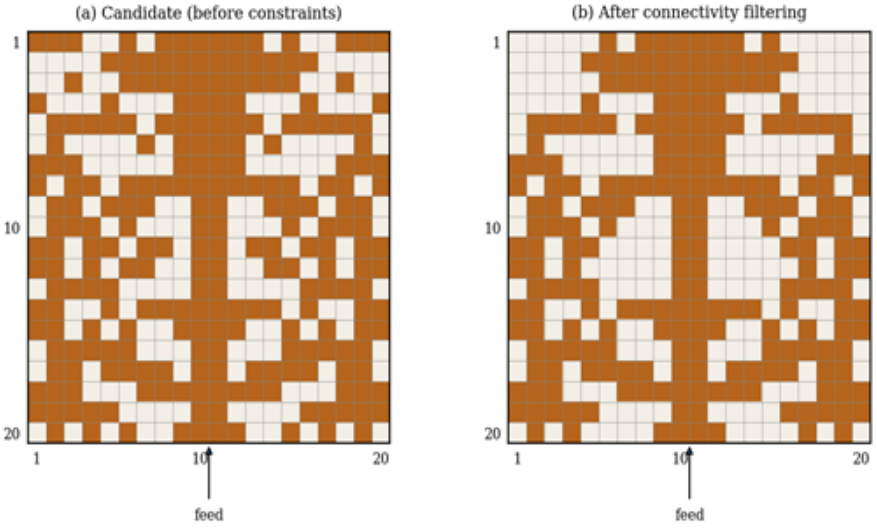


Fig. 3. Example 20 × 20 pixel encoding: (a) symmetric random candidate, (b) the same layout after removing cells not connected to the feed.

B. *Dataset Generation*

Training data are produced by co-simulation. MATLAB R2022a or Python scripts generate pixel matrices, write them into a parameterized model in CST Studio Suite 2021, run the solver and read back S_{11} over the band, realized gain, radiation efficiency and derived VSWR and bandwidth. The baseline study used 150,000 samples on a 10 × 10 grid [21]; for the larger 20 × 20 space a dataset of the order of 200,000 samples is planned, divided into training, validation and test subsets. Sampling is biased toward symmetric and feed-connected layouts, which concentrates effort on the manufacturable part of the space.

Copyright © 2026 IJEIR, All right reserved

C. *Hybrid CNN–Vision Transformer surrogate*

The surrogate architecture is shown in Fig. 4. Three convolutional blocks with batch normalization and GELU activation process the 20 × 20 input. The second and third blocks use a stride of 2, reducing the map to 5 × 5 with 128 channels. These layers capture local features such as slot edges, narrow bridges and current-crowding regions. The 5 × 5 map is then flattened into 25 tokens, a learnable positional embedding is added, and the sequence passes through four Transformer encoder layers with eight attention heads [24]. Each head computes,

$$Attention(Q,K,V) = softmax\left(\frac{QK^T}{\sqrt{d_k}}\right)V \tag{7}$$

where Q, K and V are the query, key and value projections of the tokens and d_k is the key dimension. Self-attention lets the model relate any region of the patch to any other in a single layer, which is how the network represents coupling between, for example, an arm tip and the feed junction. The encoder output is pooled and passed to a shared 256-unit layer that feeds four heads: the S_{11} curve sampled across the band, peak gain, radiation efficiency, and VSWR with bandwidth.

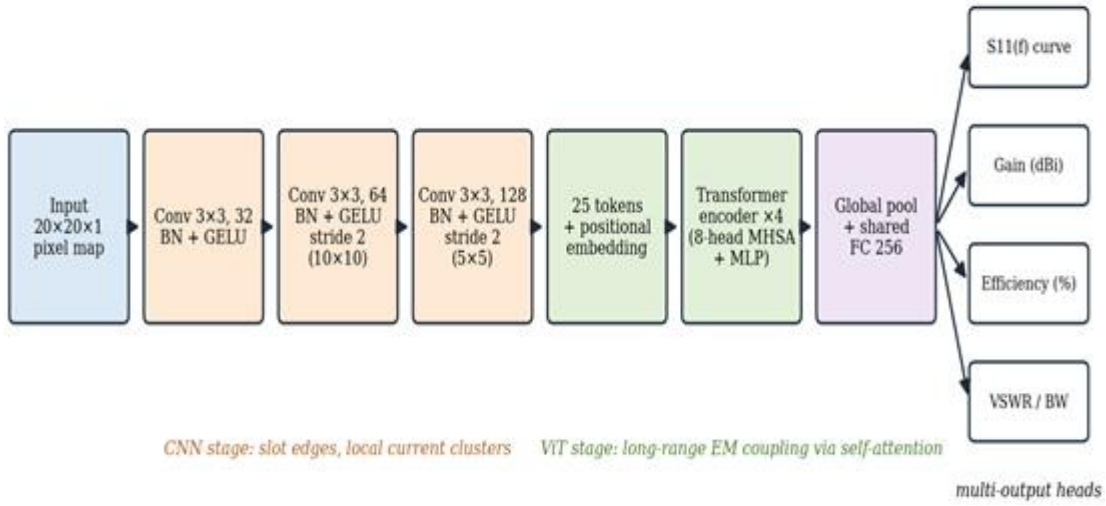


Fig. 4. Architecture of the hybrid CNN–Vision Transformer surrogate with multi-output heads.

D. *Physics-Informed Training Loss*

A purely data-driven loss can reward layouts that score well numerically but are impractical, such as checkerboard patterns. Following the physics-informed learning principle [28], the training loss is

$$\mathcal{L}_{total} = \mathcal{L}_{data} + \lambda_1\mathcal{L}_{sym} + \lambda_2\mathcal{L}_{conn} + \lambda_3\mathcal{L}_{match} \tag{8}$$

where $\mathscr{L}_{\text{data}}$ is the mean squared error between predicted and simulated outputs, $\mathscr{L}_{\text{sym}}$ penalizes departure from mirror symmetry about the feed axis, $\mathscr{L}_{\text{conn}}$ penalizes metal cells disconnected from the feed, and $\mathscr{L}_{\text{match}}$ penalizes predicted input mismatch in the target bands. The symmetry term is

$$\mathcal{L}_{sym} = \frac{1}{N}\sum_{m=1}^{20}\sum_{n=1}^{20}|p_{m,n} - p_{m,21-n}| \tag{9}$$

with N = 400. The weights λ_1, λ_2 and λ_3 are tuned on the validation set. Surrogate accuracy is assessed with the coefficient of determination R^2 and the root mean square error (RMSE) on the held-out test set.

Copyright © 2026 IJEIR, All right reserved

E. *Adaptive quantum binary PSO*

In quantum-behaved PSO [26], particles do not carry an explicit velocity. For a swarm of M particles, the mean of the personal best positions is

$$mbest = \frac{1}{M}\sum_{i=1}^{M} pbest_i \tag{10}$$

and each particle is drawn toward a local attractor that blends its personal best with the global best,

$$\varphi_{ij} = \varphi\, pbest_{ij} + (1-\varphi) gbest_j \tag{11}$$

where φ is uniformly distributed in (0, 1). The continuous position is updated as

$$x_{ij}(t+1) = \varphi_{ij} \pm \beta(t)\,|mbest_j - x_{ij}(t)|\,ln\left(\frac{1}{u}\right) \tag{12}$$

with u uniform in (0, 1). The contraction–expansion coefficient β controls the balance between exploration and exploitation. In the adaptive form used here it decreases with iteration t,

$$\beta(t) = \beta_{max} - (\beta_{max} - \beta_{min})\,\frac{t}{T} \tag{13}$$

and is additionally reset toward β_{max} whenever swarm diversity falls below a threshold, which counters the premature convergence observed with standard BPSO. Binary pixel states are recovered through a sigmoid transfer function [25],

$$p_{ij} = \{1, if\ r < \frac{1}{1+e^{-x_{ij}}};\ \ 0, otherwise \tag{14}$$

where r is uniform in (0, 1). Each particle therefore represents one 400-pixel layout, and its fitness is evaluated by the surrogate in milliseconds instead of by a full-wave solver.

F. *Multi-Objective Formulation with NSGA-II*

Gain, bandwidth and matching generally conflict, so the design is posed as the vector minimization.

$$min\ F(P) = [max\ S_{11}(f_1, f_2), -G, -\eta, -BW] \tag{15}$$

subject to the connectivity and symmetry constraints, where G is the peak realized gain, η the radiation efficiency and BW the −10 dB bandwidth. After each AQBPSO update, the combined population is ranked by NSGA-II non-dominated sorting and crowding distance [27]. Non-dominated particles form an external archive from which the global best is chosen, so the swarm moves along the Pareto front rather than toward a single weighted optimum [12]. A small number of designs from the final front are re-simulated in HFSS for verification.

V. Results and Discussion

This section first presents the full-wave results of the T-shaped reference antenna and then discusses the expected performance of the inverse design framework relative to the baseline.

A. *Reflection Coefficient and Impedance Bandwidth*

Fig. 5 shows the simulated S_{11}. Two well-defined resonances appear: −19.36 dB at 3.4125 GHz and −22.45 dB at 5.0125 GHz. Reading the −10 dB crossings from the curve, the lower band extends from about 3.27 GHz

Copyright © 2026 IJEIR, All right reserved

to 3.55 GHz, a fractional bandwidth of approximately 8.1 %, which covers the central portion of the 5G n78 allocation. The upper band begins at about 4.81 GHz and remains below −10 dB up to about 6.64 GHz, a fractional bandwidth of approximately 32 %. Between the bands, S_{11} rises to about −2.2 dB near 4.15 GHz, giving clear isolation between the two operating regions. A secondary dip near 5.35 GHz merges with the main 5.01 GHz resonance and is responsible for the broad upper band.

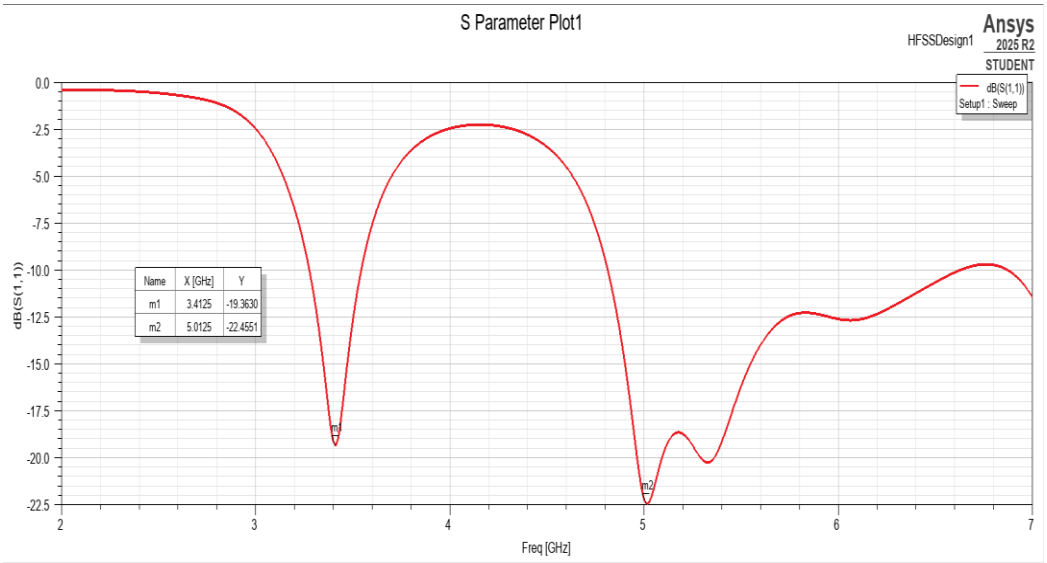


Fig. 5. Simulated reflection coefficient S_{11} of the T-shaped antenna (markers m1 and m2 at the two resonances).

The reflection coefficient and VSWR are related through

$$VSWR = \frac{1+|\Gamma|}{1-|\Gamma|}, \quad |\Gamma| = 10^{S_{11}/20} \tag{16}$$

Applying (16) to the two minima gives VSWR values of 1.24 and 1.16 and mismatch losses of only 0.05 dB and 0.03 dB. The simulated VSWR in Fig. 6 confirms the result: VSWR falls below 2 across both bands and reaches its minima at the two resonant frequencies, while it rises to about 7.7 around 4.15 GHz between the bands. Table 3 summarizes the impedance characteristics.

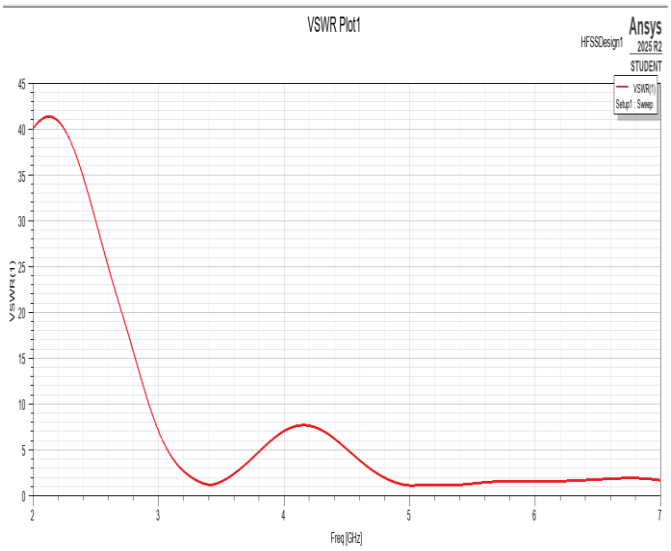


Fig. 6. Simulated VSWR of the T-shaped antenna from 2 GHz to 7 GHz.

Copyright © 2026 IJEIR, All right reserved

Table 3. Simulated impedance performance of the T-Shaped Antenna.

Parameter	Lower band	Upper band
Resonant frequency	3.4125 GHz	5.0125 GHz
Minimum S_{11}	−19.36 dB	−22.45 dB
VSWR at resonance (from (16))	1.24	1.16
−10 dB band (read from Fig. 5)	≈ 3.27–3.55 GHz	≈ 4.81–6.64 GHz
Fractional bandwidth	≈ 8.1 %	≈ 32 %
Target service	5G NR n78 (sub-6 GHz)	5 GHz WLAN / Wi-Fi

B. *Surface Current Distribution*

Fig. 7 plots the surface current magnitude on the radiator. The current is strongest along the feed and the two edges of the stem, reaching about 80 A/m near the feed junction, and it spreads into the inner halves of both arms. The arm tips carry little current at this frequency. This distribution confirms the roles assumed in Section III: the stem carries the common current that sustains both modes, and the arm segments add the electrical length that separates the two resonances. The symmetric distribution about the stem axis also indicates that the feed excites both arms equally, which is favourable for low cross-polarization.

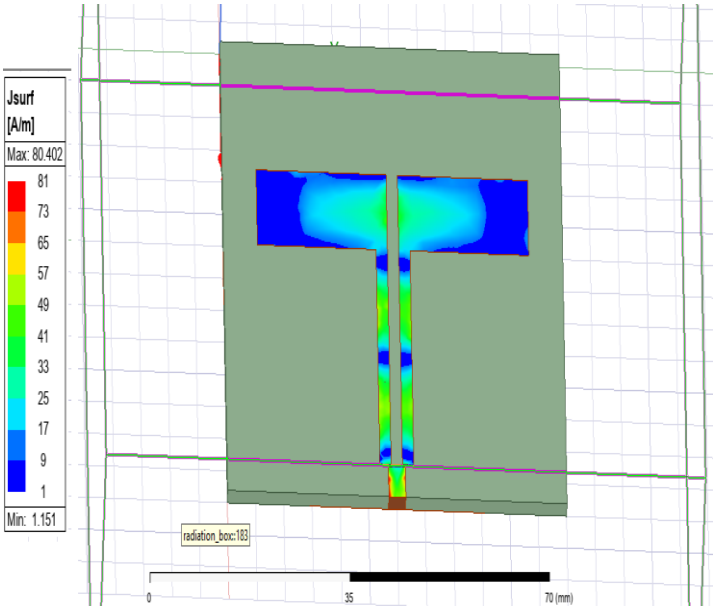


Fig. 7. Simulated surface current density (J_{surf}) on the T-shaped radiator.

C. *Gain and Radiation Pattern*

The three-dimensional total gain and far-field electric field (rE) patterns are shown in Fig. 8. Both patterns exhibit two opposing main lobes, a bidirectional shape typical of a printed radiator of this kind, with a deep null between them. The maximum of the HFSS Gain Total quantity is 2.08, which on the linear scale displayed corresponds to about 3.2 dBi, and the peak rE value is 11.1 V. The smooth, stable lobes without spurious side lobes indicate that the dual-band geometry does not distort the radiation behaviour. The moderate gain is expected for a single-layer FR4 radiator, whose dielectric loss limits efficiency; raising gain without sacrificing bandwidth is precisely the trade-off that the multi-objective framework of Section IV is designed to address.

Copyright © 2026 IJEIR, All right reserved

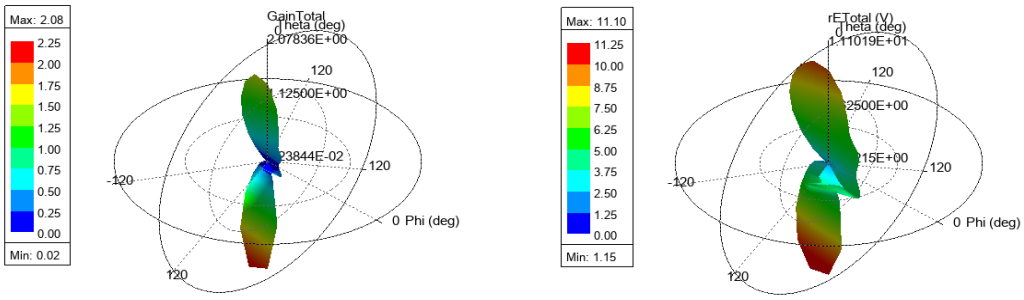


Fig. 8. Simulated three-dimensional patterns of the T-shaped antenna: (a) total gain, (b) far-field electric field rE.

D. *Expected Performance of the Inverse Design Framework*

Table 4 compares the proposed framework with the CNN–BPSO baseline [21]. The baseline reported that 500 optimization iterations required about 12.5 hours through a MATLAB-CST co-simulation loop but only about 30 minutes with the trained CNN, a 25-fold gain. The proposed framework is projected to improve this to 35-45 times, because a single surrogate call replaces several separate solver evaluations for the five predicted quantities and the adaptive swarm needs fewer iterations to converge. The design targets for the optimized antenna are a peak gain of up to 8.2 dBi and radiation efficiency of up to 99 %, with surrogate accuracy of R^2 = 0.97–0.99 and RMSE of 0.18-0.22 on the test set. These values are design targets for the ongoing implementation and will be verified by full-wave simulation of the synthesized layouts.

Table 4. Comparison of the existing and proposed design frameworks.

Feature	**CNN–BPSO baseline [21]**	**Proposed framework**
Grid resolution	10 × 10 (2^{100} layouts)	20 × 20 (2^{400} layouts)
Surrogate	CNN	Hybrid CNN–Vision Transformer
Feature scope	Local	Local and global (self-attention)
Optimizer	Binary PSO	Adaptive quantum BPSO + NSGA-II
Objectives	S_{11} only	S_{11}, gain, efficiency, VSWR, bandwidth
Result type	Single optimum	Pareto-optimal set
Physical constraints	Not explicit	Symmetry, connectivity, matching penalties
Speed-up vs. full-wave loop	≈ 25× (reported)	35–45× (estimated)

The comparison shows that the main benefit of the proposed approach lies not in a single figure of merit but in widening what can be optimized: finer geometric control, explicit modelling of long-range coupling, simulta--neous treatment of several objectives and built-in manufacturability.

E. *Discussion:*

The simulated results demonstrate effective dual-band operation, with resonances at 3.4125 GHz and 5.0125 GHz, good impedance matching, and broad upper-band coverage. Surface current distribution confirms the roles of the stem and arms in supporting the two resonant modes. The bidirectional radiation pattern achieves a peak gain of approximately 3.2 dBi. The proposed hybrid CNN–Vision Transformer framework enables multi-

Copyright © 2026 IJEIR, All right reserved

objective optimization with an estimated 35–45× speed-up, while enhanced gain and efficiency remain targets requiring full-wave validation.

VI. Conclusion and Future Scope

A dual-band T-shaped microstrip antenna on a 70 mm × 45 mm × 1.6 mm FR4 substrate has been designed and analysed in ANSYS HFSS. The antenna resonates at 3.4125 GHz and 5.0125 GHz with reflection coefficients of −19.36 dB and −22.45 dB, provides −10 dB bandwidths of approximately 3.27-3.55 GHz and 4.81-6.64 GHz, keeps VSWR below 2 in both bands and radiates stable bidirectional patterns. These characteristics make it suitable for 5G n78 and 5 GHz WLAN terminals.

Building on this reference, an inverse design framework has been formulated that encodes the radiator as a 20 × 20 pixel matrix, learns its multi-parameter response with a hybrid CNN-Vision Transformer surrogate trained under physics-informed constraints, and explores the design space with adaptive quantum binary PSO combined with NSGA-II. Relative to the existing 10 × 10 CNN–BPSO method, the framework extends optimization from S_{11} alone to gain, efficiency, VSWR and bandwidth, and it is projected to shorten design time by 35-45 times compared with direct full-wave optimization.

Future work will complete the training dataset and surrogate, verify the Pareto-optimal layouts by full-wave simulation and fabrication, and measure the prototypes. Further directions include low-loss substrates and small arrays to raise gain, material-dependent inputs to improve surrogate generalization, reconfigurable pixel switching, and extension of the method toward millimetre-wave and terahertz bands for 6G and satellite links.

References

[1] 3GPP, "NR; User Equipment (UE) radio transmission and reception; Part 1: Range 1 standalone," 3GPP TS 38.101-1.
[2] IEEE Standard for Information Technology-Telecommunications and Information Exchange between Systems, Local and Metropolitan Area Networks-Specific Requirements, Part 11, Amendment 1: Enhancements for High-Efficiency WLAN, IEEE Std 802.11ax-2021, 2021.
[3] N. Chhaule et al., "A comprehensive review on conventional and machine learning-assisted design of 5G microstrip patch antenna," Electronics, vol. 13, Art. no. 3819, 2024.
[4] C. A. Balanis, Antenna Theory: Analysis and Design, 4th ed. Hoboken, NJ, USA: Wiley, 2016.
[5] R. Garg, P. Bhartia, I. Bahl, and A. Ittipiboon, Microstrip Antenna Design Handbook. Norwood, MA, USA: Artech House, 2001.
[6] F.-C. Chen et al., "A series-fed slant-polarized microstrip patch antenna array," IEEE Transactions on Antennas and Propagation, pp. 5367–5372, 2024.
[7] N. Ou et al., "Wideband, dual-polarized patch antenna array fed by novel, differentially fed structure," Electronics, vol. 13, Art. no. 1382, 2024.
[8] Z. Ji et al., "A wideband circularly polarized complementary antenna for millimeter-wave applications," IEEE Transactions on Antennas and Propagation, pp. 2392–2400, 2022.
[9] X. Yi et al., "Wideband and high-gain substrate integrated folded horn fed open slot antenna," IEEE Transactions on Antennas and Propagation, pp. 2602–2612, 2022.
[10] R. Shi et al., "Simple E-plane decoupling structure using embedded mushroom element for wide-angle scanning linear microstrip phased arrays," IEEE Antennas and Wireless Propagation Letters, pp. 339–343, 2025.
[11] G.-H. Sun et al., "A hollow-waveguide-fed planar wideband patch antenna array for terahertz communications," IEEE Transactions on Terahertz Science and Technology, pp. 10–19, 2023.
[12] N. Jin and Y. Rahmat-Samii, "Advances in particle swarm optimization for antenna designs: Real-number, binary, single-objective and multiobjective implementations," IEEE Transactions on Antennas and Propagation, vol. 55, no. 3, pp. 556–567, Mar. 2007.
[13] H. M. El Misilmani, "Machine learning in antenna design: A comprehensive overview," IEEE Access, pp. 103890–103915, 2023.
[14] Q. Wu et al., "Machine-learning-assisted optimization for antenna geometry design," IEEE Transactions on Antennas and Propagation, pp. 2083-2095, 2024.
[15] L.-Y. Xiao et al., "Inverse artificial neural network for multiobjective antenna design," IEEE Transactions on Antennas and Propaga--tion, pp. 6651-6659, 2021.
[16] A. Gupta et al., "Tandem neural network based design of multiband antennas," IEEE Transactions on Antennas and Propagation, pp. 6308-6317, 2023.
[17] J. P. Jacobs, "Convolutional neural-network regression for dual-band pixelated microstrip antennas," IEEE Antennas and Wireless Propagation Letters, pp. 2417-2421, 2021.
[18] E. A. Karahan et al., "Deep learning-based inverse design for planar antennas at RF and millimeter-wave," in Proc. IEEE International Symposium on Antennas and Propagation, 2022.
[19] E. A. Karahan et al., "Deep-learning-based inverse-designed millimeter-wave passives and power amplifiers," IEEE Journal of Solid-State Circuits, pp. 3074-3088, 2023.

Copyright © 2026 IJEIR, All right reserved

[20] O. Noakoasteen et al., "GAN-based synthetic data generation for antenna design," IEEE Open Journal of Antennas and Propagation, pp. 488-494, 2022.
[21] S. Chen et al., "Inverse design of microstrip antennas based on deep learning," Electronics, vol. 14, Art. no. 2510, 2025.
[22] Z. Du et al., "An optimization design method for dual-band and wideband patch filtering power dividers," Electronics, vol. 13, Art. no. 528, 2024.
[23] A. Vaswani et al., "Attention is all you need," in Proc. Advances in Neural Information Processing Systems (NeurIPS), 2017, pp. 5998–6008.
[24] A. Dosovitskiy et al., "An image is worth 16x16 words: Transformers for image recognition at scale," in Proc. International Conference on Learning Representations (ICLR), 2021.
[25] J. Kennedy and R. C. Eberhart, "A discrete binary version of the particle swarm algorithm," in Proc. IEEE International Conference on Systems, Man, and Cybernetics, 1997, vol. 5, pp. 4104-4108.
[26] J. Sun, B. Feng, and W. Xu, "Particle swarm optimization with particles having quantum behavior," in Proc. IEEE Congress on Evolutionary Computation, 2004, pp. 325-331.
[27] K. Deb, A. Pratap, S. Agarwal, and T. Meyarivan, "A fast and elitist multiobjective genetic algorithm: NSGA-II," IEEE Transactions on Evolutionary Computation, vol. 6, no. 2, pp. 182-197, Apr. 2002.
[28] M. Raissi, P. Perdikaris, and G. E. Karniadakis, "Physics-informed neural networks: A deep learning framework for solving forward and inverse problems involving nonlinear partial differential equations," Journal of Computational Physics, vol. 378, pp. 686-707, 2019.

AUTHOR'S PROFILE



Lakshmi Ganabathy A, received the B.E in Electronics and Communication Engineering from Anna University. He is currently pursuing the Master of Technology (M.Tech, part-time) degree in Communication Systems in the Department of Electronics and Communication Engineering, Ponnaiyah Ramajayam Institute of Science and Technology (PRIST) Deemed to be University, Thanjavur, Tamil Nadu, India. Lecturer at SDS polytechnic college with more than 4 years of experience, Research interests include microstrip and reconfigurable antenna design, electromagnetic simulation, and the application of deep learning and swarm intelligence to RF and antenna engineering.

Copyright © 2026 IJEIR, All right reserved